Dalton Transactions

Accepted Manuscript

Volume 46
Number 10
14 March 2017
Pages 3073-3412

Dalton Transactions

An international journal of inorganic chemistry

rsc.li/dalton

ISSN 0306-0012

COMMUNICATION
Douglas W. Stephan et al
N-Heterocyclic carbene stabilized parent sulfenyl, selenenyl, and tellurenyl cations (XH+; X = S, Se, Te)

This is an Accepted Manuscript, which has been through the Royal Society of Chemistry peer review process and has been accepted for publication.

Accepted Manuscripts are published online shortly after acceptance, before technical editing, formatting and proof reading. Using this free service, authors can make their results available to the community, in citable form, before we publish the edited article. We will replace this Accepted Manuscript with the edited and formatted Advance Article as soon as it is available.

You can find more information about Accepted Manuscripts in the Information for Authors.

Please note that technical editing may introduce minor changes to the text and/or graphics, which may alter content. The journal's standard Terms & Conditions and the Ethical guidelines still apply. In no event shall the Royal Society of Chemistry be held responsible for any errors or omissions in this Accepted Manuscript or any consequences arising from the use of any information it contains.

ROYAL SOCIETY OF CHEMISTRY

rsc.li/dalton

Ligand Modification for the Tuning of Activity and Selectivity in Chemoselective Transfer Hydrogenation of α,β-Unsaturated Carbonyls using EtOH as Hydrogen Source

Alicia Beaufils,[a] Nicole Elia,[a] Sabela Reuge,[a] and Martin Albrecht*,[a]

Department of Chemistry, Biochemistry, and Pharmaceutical Sciences, University of Bern, Freiestrasse 3,

CH-3012 Bern (Switzerland)

E-Mail: martin.albrecht@unibe.ch

Abstract: The selective reduction of α,β-unsaturated ketones either at the olefinic or the carbonyl site offers attractive synthetic opportunities. While carbonyl reduction is well established, selective olefin reduction is less common, particularly when using environmentally friendly ethanol as hydrogen source. Recently, we reported a coordinatively unsaturated ruthenium complex containing a *N,N'*-bidentate coordinating pyridinium amidate (PYA) ligand as an efficient catalyst for ethanol-based transfer hydrogenation of α,β-unsaturated ketones, however with overreduction and thus loss of selectivity in reactions over an extended period of time. Capitalizing on the facile synthetic modulation of PYA ligands, we here report on a series of operationally unsaturated two-legged piano-stool ruthenium cymene complexes [Ru(N^N')(cym)](PF$_6$) **3a–e** with modifications on the PYA-appended aroyl unit. Spectroscopic analysis of these complexes suggest a higher contribution of the π-basic zwitteronic resonance structure of the PYA unit in CD$_2$Cl$_2$ and a larger contribution of the π-acidic quinoidal structure in polar and more coordinating CD$_3$OD. The latter also allows for stabilization of catalytically relevant alkoxide intermediate [Ru(OEt)(N^N')(cym)] **4**. Application of complexes **3a–3e** in transfer hydrogenation of *trans*-chalcone indicates generally good transfer hydrogenation activity and good selectivity towards olefin hydrogenation for all complexes. The variant with a p-CF$_3$-C$_6$H$_4$ substituted PYA ligand, complex **3c**, combined high activity and very high selectivity, affording almost exclusively the desired saturated ketone product with only traces of the saturated alcohol even after prolonged reaction times, underpinning the effectiveness of PYA ligand modulation to tailor activity and selectivity.

Introduction

Metal-mediated catalysis is relying on the availability of a free coordination site at the metal center for substrate coordination.[1–3] In homogeneous catalysis, such a free site can be introduced by various methodologies, including the cleavage of dimeric complexes or the selective abstraction of a coordinated ligand. The later method often involves solvent coordination,[4] and thus ligand abstraction typically results in the replacement of a kinetically robust ligand by a kinetically labile one. In some cases, however, coordinative unsaturation is sufficiently stable for 'under-ligated' complexes to be isolated,[5–8] with obvious opportunities for catalysis. Closer inspection of such coordinatively unsaturated complexes indicated that one of the ligands tends to compensate the unsaturation by π-donor interactions, which leads to partial electronic saturation.[9–11] As a consequence, the term 'operationally unsaturated' has been proposed to characterize these complexes.[8,11,12]

We recently demonstrated that functionalized and bidentate coordinating pyridinium amidate (PYA) ligands[13] readily form operationally unsaturated complexes of iridium(III) and ruthenium(II), leading to compounds with two-legged piano-stool geometries such as **I** and **II** (Fig. 1a).[14–17] These complexes are sufficiently stable to be isolated in the solid state and for investigation of their reactivity towards exogeneous ligands and substrates for catalytic transformations.[16,17] For example, the PYA iridium complex **I** is a catalyst for formic acid dehydrogenation with outstanding activity,[14] while ruthenium complex **II** efficiently catalyzes the transfer hydrogenation of α,β-unsaturated ketones under mild conditions using ethanol as a renewable and attractive hydrogen source.[18] Despite their high efficiency, the hydrogen transfer led to gradual over-reduction of the C=O bond after complete transformation of the olefinic C=C bond, thus limiting its applicability since quenching of the reaction at full conversion is necessary to maintain high selectivity. This limitation prompted us to investigate the implication of the ligand system in order to suppress the undesired carbonyl reduction reactivity.
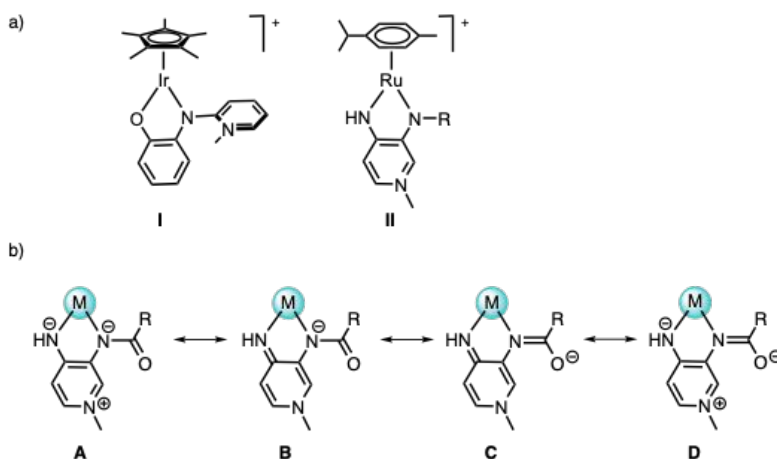
Figure 1. a) Underligated Ir^{III} and Ru^{II} complexes containing pyridinium amidate (PYA) ligands; b) schematic representation of the limiting resonance structures in N,N'-bidentate PYA complexes.

Among the PYA ligands reported over the years,[13,19–24] one influential variation on the ligand scaffold pertains to the acyl unit. For example, carbonyl substituents incorporating donor motifs such as pyridine, N-heterocyclic carbene, or phenyl group as chelating ligands have been developed.[25–28] Taking advantage of the specific N,N'-coordination of the ligand and the easy modification of PYAs,[13] we describe here the synthesis and characterization of a series of N,N'-bidentate PYA ruthenium complexes derived from **II** with modified acyl units. The flexible donor properties of the N,N'-bidentate PYA unit are represented by the various limiting resonance structures including (i) coordination as formally dianionic π-basic ligand with remote pyridinium stabilization (resonance structure **A**, Fig. 1b) and (ii) as a formally monoanionic ligand with a π-acidic ligand imine-type coordination site (resonance structures **B**, **D**). In addition, we envisioned that the acyl substituent R further affects the electronic properties of the metal center, with the possibility to introduce two formally neutral imine bonding sites and a remote oxoanionic feature as shown in the limiting resonance structure **C**. Such electronic modulation in the acyl unit was previously demonstrated to affect metal coordination with first-row pincer-type PYA complexes, though with a change in the amide coordination mode from nitrogen (κ-N) to oxygen (κ-O).[29] Furthermore, steric effects at this position are expected to influence the accessibility of the metal center by the substrate, thus impacting both activity and selectivity, a common challenge for transfer hydrogenation of α,β-unsaturated ketones.[30–33] Here we have explored the impact of

systematic acyl modifications on the catalytic application of N,N-bidentate PYA ruthenium complexes in

transfer hydrogenation using ethanol as hydrogen source. Specifically, we demonstrate that specific

variations of the acyl unit enhance the selectivity towards olefin reduction considerably, even in reactions that

were run over extended time periods.

Results and discussion

Synthesis and characterization of second-generation of *N,N'*-bidentate PYA ruthenium complexes

The ligand precursor pyridinium salts were synthesized according to previously reported procedures,[16]

starting from *tert*-butyl(3-amino-pyridin-4-yl)carbamate and substituted acyl chlorides (Scheme 1). The acyl

chlorides were commercially available except for 4-methoxy-1-naphthoyl chloride, which was synthesized in

quantitative yield from the corresponding carboxylic acid in the presence of an excess of $SOCl_2$. Amidation of

these acyl chlorides under basic conditions yielded compounds **1a–e** in acceptable 54–90% yields. In the

presence of 5 eq of MeOTf, selective methylation of the pyridine nitrogen accompanied with Boc-deprotection

of the 4-amino sites yielded the corresponding pyridinium salts **2a–e**. Direct anion exchange from OTf⁻ to PF_6^-

was performed for complexes **2a** and **2b** and was accomplished with an excess of NH_4PF_6 in a $MeCN/H_2O$

mixture. While the triflate salt of **2b** was isolated as an oil, the PF_6^- analogue was obtained as a solid, which

facilitated purification considerably. An attempt to expand the aryl substituent to anthracyl groups failed

because methylation of **1g** gave only decomposition products irrespective of the methylating agent (MeOTf

or MeI), or the reaction conditions (25–40°C, CH_3CN or CH_2Cl_2 as solvent, 1–5 eq MeX) and yielded the

starting compound pyridine-3,4-diamine as the major product. Salts **2a–b** were ruthenated in the presence of

$[RuCl_2(cym)]_2$ (cym = p-cymene) and NaOAc in CH_2Cl_2 under reflux conditions, and with the addition of $NaPF_6$

for salts **2c–e** to afford the corresponding air- and moisture-stable complexes **3a–e** in 66–92% yield.

Remarkably, ruthenation of ligand **2f** with a methyl rather than an aryl substituent led to a mixture of products,

which was not followed up any further. Successful formation of the ruthenium complexes **3a–e** was indicated

macroscopically by a change of color of the reaction mixture from light to dark red and was confirmed by

mass spectrometry and elemental analysis. Evidence for the formation of complexes **3a–e** was obtained by

^{1}H NMR spectroscopy, with loss of the amide proton resonance and strong deshielding of the NH singlet integrating for one proton only. Moreover, diagnostic shifts of the PYA proton resonances indicate metal coordination. While the pyridylidene protons $H_{\alpha'}$ and H_β shifted downfield upon ruthenation, the pyridylidene proton H_α of all complexes **3a–e** resonates at noticeably higher field compared to the same nucleus in ligand precursors **2a–e** ($\Delta\delta$ about –0.5 ppm).
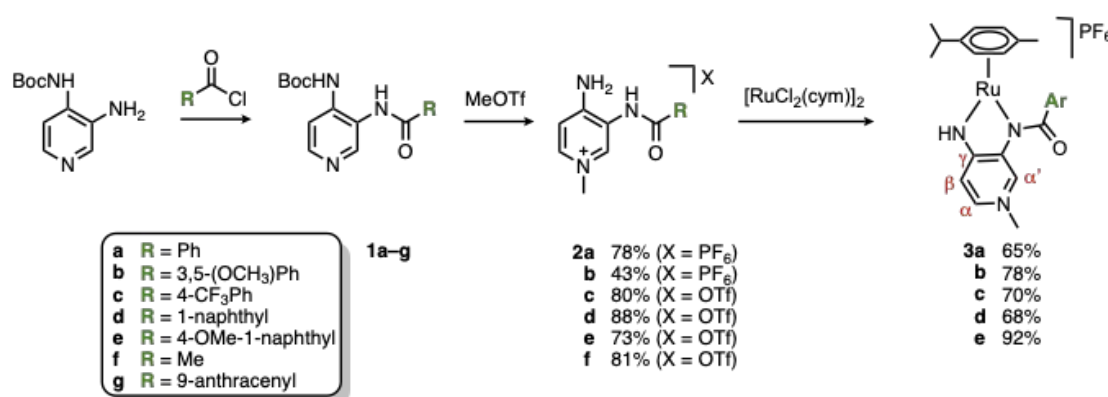
Scheme 1. Synthesis of ligands and ruthenium complexes **3a–e**.

Spectroscopic and structural analysis of complexes 3a–e

The electronically flexible character of the PYA ligand imparts stability to the formally underligated complex, predominantly through π-donation via enhanced contribution of the zwitterionic structure **A** (Fig. 1b), while π-acidic bonding through resonance forms **B** and **C** promotes the coordination of an additional ligand L to attain the more common three-legged piano-stool ruthenium geometry.[16] The chemical shift difference between pyridylidene protons H_α and H_β (*cf.* Scheme 1) is a diagnostic probe to evaluate the electronic structure of the ligand, with larger values indicating higher contribution of the quinoidal form **B**.[34] Analysis of the chemical shifts of the PYA H_α, $H_{\alpha'}$ and H_β protons of complexes **3a–e** indicates a similar ligand electronic structure that is independent of the acyl substituent when measured in CD_2Cl_2, a low-polarity solvent (Table 1, entries 1–5). The $\Delta(H_\alpha-H_\beta)$ is 0.10(3) ppm and very similar in all complexes. The most notable difference pertains to $H_{\alpha'}$, which is considerably more deshielded in complexes **3d** and **3e** (δ_H = 9.22 and 8.94, respectively) in comparison to the frequencies observed for complexes **3a–c**, δ_H = 8.56 (±0.01). This deshielding has been tentatively attributed to a more defined orientation of the naphthyl substituents compared to the phenyl

analogues and ensuing hydrogen bonding of the carbonyl oxygen with $H_{\alpha'}$. When the ^{1}H NMR analyses were performed in CD_3OD instead of CD_2Cl_2, a significant increase of the chemical shift differences of these pyridylidene protons to $\Delta(H_{\alpha}-H_{\beta}) = 0.46(3)$ ppm was observed (entries 6–10). These changes are beyond regular solvent effects as judged by the minor displacement of the cymene signals (Table S1). The larger shift difference in CD_3OD for complexes **3a–e** therefore suggests a higher contribution of the quinoidal form **B** in polar methanol. Notably, the opposite trend is generally observed, *i.e.* larger contribution of zwitterionic ligand structure **A** in polar solvents.[25,34,35] This opposite trend observed here with complexes **3a–e** is similar to that of cognate coordinatively unsaturated iridium PYA complexes.[17] It has been attributed to reversible solvent coordination leading to a higher electron density at the metal center by the additional solvento ligand. The higher electron density imparted by a σ-bound solvento ligand alleviates the requirement for a strongly π basic PYA structure to stabilize the metal center, and thus leads to a higher predominance of the quinoidal ligand structure **B** (or **C**). In contrast, with coordinatively saturated complexes, the polarity of the solvent (rather than its coordination ability) generally leads to a preponderance of the zwitterionic structure.

Table 1 Selected ^{1}H NMR shifts (ppm) of the CH_{α}, $CH_{\alpha'}$, CH_{β} units for complexes **3** and **4**.

entry	complex	solvent	$H_{\alpha'}$	H_{α}	H_{β}	$\Delta(H_{\alpha'}-H_{\beta})$	$\Delta(H_{\alpha}-H_{\beta})$
1	**3a**	CD_2Cl_2	8.55	7.35	7.28	1.27	0.07
2	**3b**	CD_2Cl_2	8.55	7.34	7.25	1.30	0.09
3	**3c**	CD_2Cl_2	8.57	7.38	7.30	1.27	0.08
4	**3d**	CD_2Cl_2	9.22	7.42	7.29	1.93	0.13
5	**3e**	CD_2Cl_2	8.94	7.38	7.28	1.66	0.10
6	**3a**	CD_3OD	8.67	7.61	7.18	1.49	0.43
7	**3b**	CD_3OD	8.70	7.58	7.15	1.55	0.43
8	**3c**	CD_3OD	8.76	7.58	7.09	1.67	0.49
9	**3d**	CD_3OD	9.28	7.98	7.12	2.16	0.86
10	**3e**	CD_3OD	9.03	7.66	7.20	1.83	0.46
11	**4a**	CD_3OD	8.91	7.28	6.63	2.28	0.65

12	**4b**	CD$_3$OD	8.96	7.12	6.38	2.58	0.74
13	**4c**	CD$_3$OD	9.07	7.14	6.40	2.67	0.74
14	**4d**	CD$_3$OD	9.26	7.17	6.42	2.84	0.75

Preliminary mechanistic studies of the catalytic transfer hydrogenation with complex **3a** using EtOH as benign hydrogen source[36–40] suggested the formation of the alkoxide complexes **4** as an initially formed species (Scheme 2). Alkoxide coordination to complexes **3a–d** was accomplished with NaOEt in CD$_3$OD on the NMR scale. Coordination of an anionic ligand induced an even larger separation of H$_\alpha$ and H$_\beta$ protons $\Delta(H_\alpha–H_\beta)$ = 0.70(5) ppm (Table 1, entries 11–14; Fig. 2), further showcasing the higher contribution of the quinoidal resonance form upon coordination of an anionic ligand as a consequence of the higher electron density at the ruthenium center.[16] These NMR spectroscopic data therefore underpin the electronically dynamic character of the PYA system (*cf* Fig. 1b), with a higher contribution of the quinoidal resonance form **B** in coordinating solvents, which is particularly useful to generate and stabilize the catalytically relevant intermediate **4**.
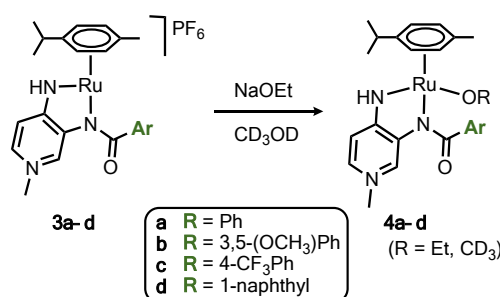
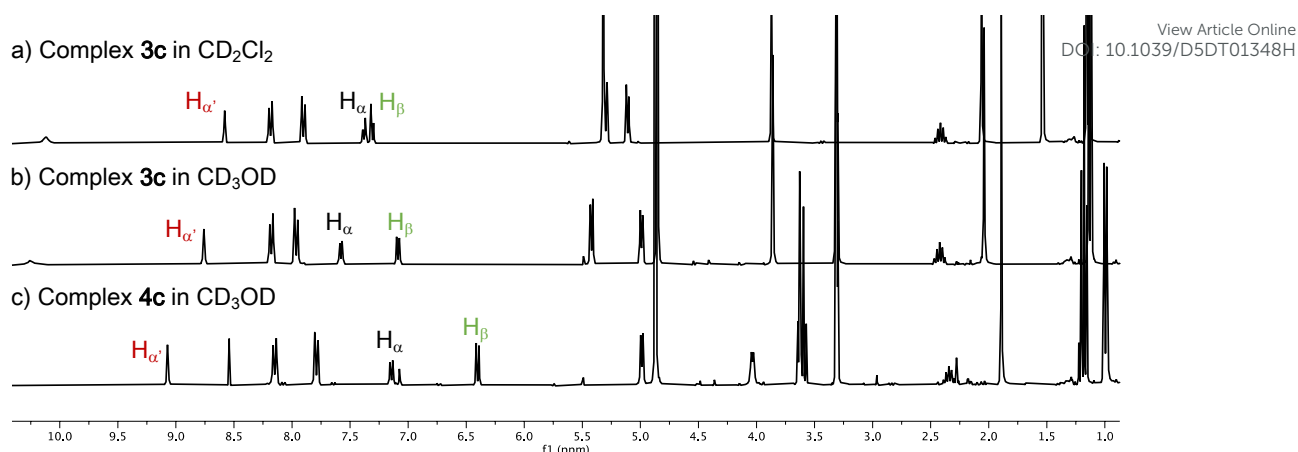**Scheme 2.** Synthesis of the alkoxide ruthenium complexes **4a–d**.

Figure 2. Stacked ^{1}H NMR spectra (298 K, 300 MHz) of a) complex **3c** in CD$_2$Cl$_2$, b) **3c** in CD$_3$OD, and c) **4c** in CD$_3$OD, showing the chemical shift of pyridylidene protons H$_\alpha$, H$_{\alpha'}$, and H$_\beta$.

While UV-Vis spectroscopy has been used to probe the donor strength of the ligand system,[25] no significant trends were observed for complexes **3a–e**. All complexes show a diagnostic metal-to-ligand charge transfer (MLCT) band in the visible region with an absorption maximum λ_{max} = 410±1 nm (Fig. 3, Table S2). The similarity of the absorption maxima is in agreement with the essentially identical chemical shifts of the PYA protons for complexes **3a–e**, suggesting no impact of the acyl modification on the PYA donor properties. Rather remarkably, the absorption maximum is identical in CH$_2$Cl$_2$ and in CH$_3$OH (Fig. S1), indicating no major solvent-dependence in contrast to the NMR spectroscopic data. The solvent independence of the absorption band may point to non-PYA orbitals orbitals involved in the lowest energy transition.[41,42] Electrochemical analysis of complex **3a** by cyclic voltammetry revealed several processes, some (quasi-)reversible *e.g.* at $E_{1/2}$ = +0.24 and +0.72 V, and others irreversible, *e.g.* at E_{pa} = +1.18 and + 1.55 V, as a consequence of a combination of ligand- and metal-centered processes (Fig. S2). The difficulty in attributing and thus rationalizing the different processes prevented us from using this technique to probe the donor strength of the ligand.
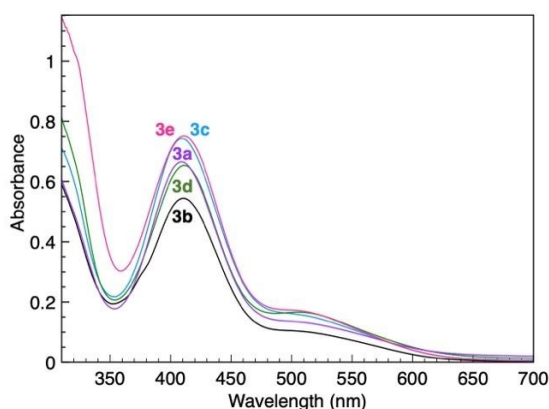
Figure 3. UV-Vis absorption spectra of Ru(II) PYA complexes **3a–e** with various acyl substituents (in CH_2Cl_2.

Suitable crystals of complex **3b** for X-ray diffraction analysis were obtained from a CH_2Cl_2/Et_2O mixture. The structure of complex **3b** revealed a two-legged piano-stool geometry in the solid state (Fig. 4). The pyramidalization angle α, defined as the angle between the centroid of the N–Ru–N moiety, the Ru center, and the centroid of the capping *p*-cymene, is a good indicator of the coordinative unsaturation of these complexes.[8] Complexes **3a** and **3b** feature a pyramidalization angle α of 176°, confirming the absence of agostic interactions between the ligand and the metal center and also confirming a monomeric structure in the solid-state (Table 2). Comparison of the bond lengths with complex **3a**, which bears a phenyl group instead of 3,5-dimethoxyphenyl, revealed a highly similar structure within the PYA system. Notably, the C1–N1 bond is in both complexes some 0.06 Å shorter than the C5–N2 bond, pointing to a larger π bond contribution to the C–N bond *para* to the N-Me site, which reinforces the relevance of a quinoidal resonance structure. While single crystals of complexes **3c** and **3e** were also grown, they did not diffract enough for a full measurement. Nonetheless, preliminary structure determination of complex **3c** showed the same two-legged piano stool structure as identified for **3b**.

Table 2. Selected bond lengths (Å) and angles (deg) in complexes **3a** and **3b**.

	complex **3a** [a]	complex **3b**
Ru1–N1	1.963(2)	1.968(2)
Ru1–N2	2.043(2)	2.044(2)
N1–C1	1.340(4)	1.338(3)
N2–C5	1.396(3)	1.396(3)
N2–C7	1.398(3)	1.399(2)
C7–O1	1.216(3)	1.216(2)
C7–C8	1.493(3)	1.500(3)

C_α–C_β [b]	1.371(8)	1.367(7)
C_β–C_γ [b]	1.415(6)	1.415(5)
N1–Ru–N2	78.63(8)	78.52
α [c]	176.55	176.75

[a] from ref 16; [b] C_α–C_β is the average bond length of C2–C3 and C4–C5, C_β–C_γ is the average bond length of C1–C2 and C1–C5; [c] pyramidalization angle α is the angle between the centroid of N–Ru–N moiety, Ru, and the centroid of p-cym.
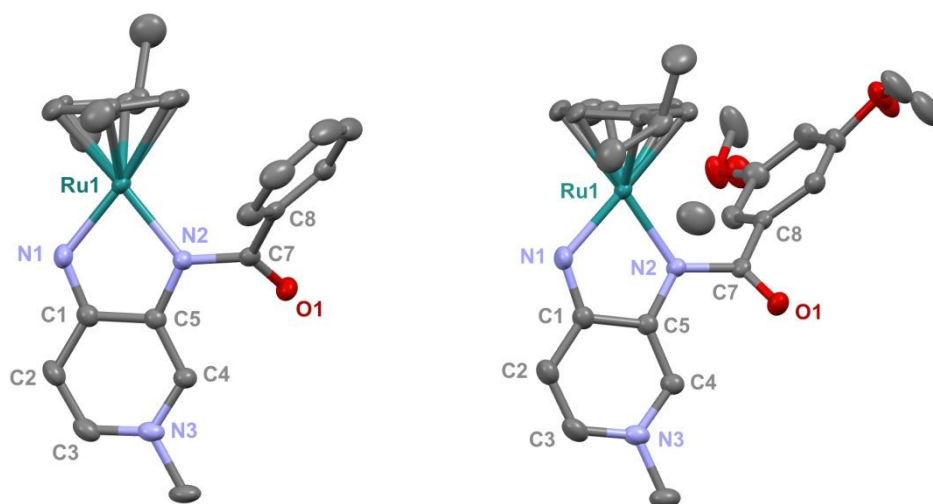

Figure 4. Molecular structure of complexes **3a** (left, from ref. 16) and **3b** (right) from X-ray diffraction (50% probability ellipsoids; hydrogen atoms and non-coordinating PF_6^- anions omitted for clarity).

Chemoselective transfer hydrogenation of α,β-unsaturated ketones. Based on the activity of **3a** in the chemoselective transfer hydrogenation of unsaturated ketones,[18] complexes **3a–e** were investigated in this reaction using *trans*-chalcone **5a** as model substrate (Table 3). Under optimized conditions, *i.e.* 1 mol% complex and 5 mol% K_2CO_3 in 5 mL EtOH at 25 °C under a N_2 atmosphere, complex **3a** achieved 78% yield of the desired saturated ketone **6a** within 1 h. Time-dependent monitoring of the conversion revealed a maximum turnover frequency $TOF_{C=C}$ = 170 h^{-1} (entry 1). The reaction rates were slower when using complexes **3b** or **3c**, which required 3 and 2 h, respectively, to reach similar yields (entries 2, 3). The most active complex of this series was the naphthalene-based complex **3d**, with a $TOF_{C=C}$ = 200 h^{-1} and achieving 97% yield of ketone **6a** in 50 min (entry 4). Similarly, 96% yield of **6a** was obtained with complex **3e** after a slightly longer reaction time of 1 h (entry 5). Further monitoring of the reaction revealed that upon full consumption of the substrate, hydrogenation of the carbonyl bond was initiated to eventually afford the fully

saturated alcohol **7a**. This second hydrogenation was slower for all catalysts tested here, as seen from the $TOF_{C=O} \leq 11$ h^{-1} (see SI for details). For example, complex **3a** accomplished 59% ketone hydrogenation in 24 h to give alcohol **7a** (Fig. 5a). Complex **3b**, which is less active in olefin hydrogenation, is also less active in carbonyl hydrogenation, yielding a modest 11% of the fully saturated product **7a** after 24 h (Fig. S3a). Complex **3c** is even slower in this second hydrogenation, and the ketone was recovered in 98% after 24 h (Fig. 5c). In sharp contrast, the fastest olefin hydrogenation using complex **3d** ($k_{C=C} = 101 \times 10^{-5}$ h^{-1}) also showed high activity towards C=O bond hydrogenation and reached 85% yield of alcohol **7a** in 24 h ($k_{C=O} = 5.5 \times 10^{-5}$ h^{-1}, Fig. S3b). Similarly, a lack of selectivity was observed with complex **3e**, with 61% of the fully hydrogenated product **7a** present after 24 h (Fig. 5e). While these data indicate good general selectivity towards olefin hydrogenation of all complexes **3a–e**, the specifity of complex **3c** stands out as it provides exclusively the ketone product with only traces of the saturated alcohol even after extended reaction times. Quantitatively, the selectivity is reflected by the ratio of the two reaction rates, Sel = $k_{C=C}$ / $k_{C=O}$. This ratio is 110 for **3c** and almost an order of magnitude higher than for the other complexes (20±5). Speculatively, the higher selectivity of **3c** may be attributed to a fine balance of π stacking behavior of the substrate **5a** *vs* the partially saturated **6a** with the electron-deficient CF$_3$-aryl unit of the catalyst (*vide infra*). In addition, the putative hydride derived from **3c** is expected to have the highest hydricity due to the electron-withdrawing character of the acyl group and the ensuing increase of the relevance of the dianionic ligand resonance structure **A**.

Table 3. Comparison of catalytic data for transfer hydrogenation of *trans*-chalcone **5a** using complexes **3a–e**.[a]
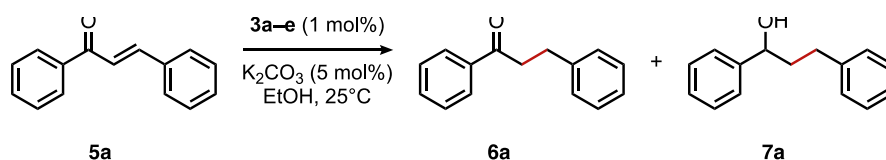
entry	complex	yield$_{max}$ **6a** (time)	**6a** : **7a** (%) (24 h)	$k_{C=C}$ (10^{-5} h^{-1})	$k_{C=O}$ (10^{-5} h^{-1})	TOF$_{C=C}$ (h^{-1})	TOF$_{C=O}$ (h^{-1})	Sel [b]
1	**3a**	98% (1 h)	41 : 59	74	3.9	170	7	19
2	**3b**	98% (3 h)	90 : 11	38	~1.5 [c]	100	2	25

3	**3c**	98% (2 h)	98 : 2	56	0.5	130	1	110
4	**3d**	97% (0.83 h)	15 : 85	101	5.5	200	11	18
5	**3e**	96% (1 h)	39 : 61	76	5.1	160	9	15

[a] Reaction conditions: *trans*-chalcone **5a** (0.5 mmol), K_2CO_3 (5 mol%), complex **3a–e** (1 mol%) in EtOH (5 mL), 25 °C, N_2; yields determined by ^{1}H NMR spectroscopy relative to 1,3,5-trimethoxybenzene from duplicate runs. R^2 for rates > 0.98; [b] Sel = selectivity = $k_{C=C}$ / $k_{C=O}$; [c] not sufficient data points for an accurate determination.
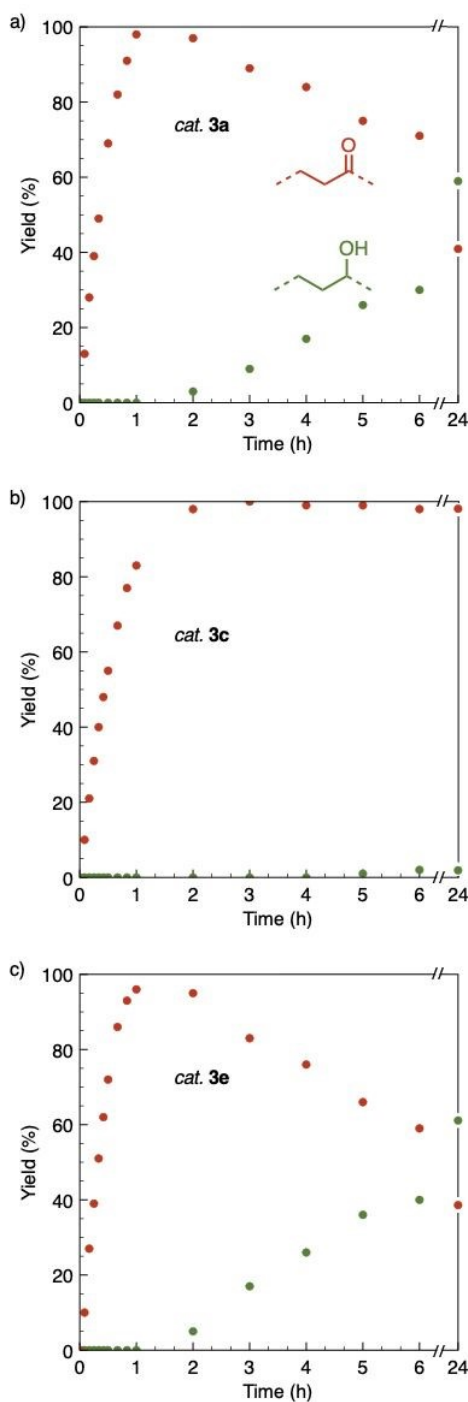
Figure 5. Time-conversion profiles of the Ru-catalyzed transfer hydrogenation of *trans*-chalcone **5a** to form subsequently 1,3-diphenylpropan-1-one (red dots) and 1,3-diphenylpropan-1-ol (green dots) using EtOH as hydrogen source and complexes **3a** (a), **3c** (b) and **3e** (c) as catalyst precursors.

This trend in ketone hydrogenation activity of complexes **3a–e** was further confirmed when using pure 1,3-diphenylpropan-1-one **6a** directly as substrate under optimized catalytic conditions (Fig. 6). In this reaction, complex **3d** provided again the most active catalyst, with 91% of alcohol **7a** after 24 h *vs* 85% starting from *trans*-chalcone (Table 4, entry 4). Moderate yields of 70% and 62% were obtained for complexes **3a** and **3e**, respectively (entries 1 and 5), and **3b** achieved only 41% yield within 24 h. This complex was also slow in olefin hydrogenation, indicating that the general catalytic activity of this complex is only modest. Complex **3c** gave the lowest activity towards C=O bond hydrogenation, with 14% yield of alcohol product **6a** after 24 h,[43] thus supporting the poor interaction of the complex with the saturated ketone once olefin hydrogenation took place (see above).
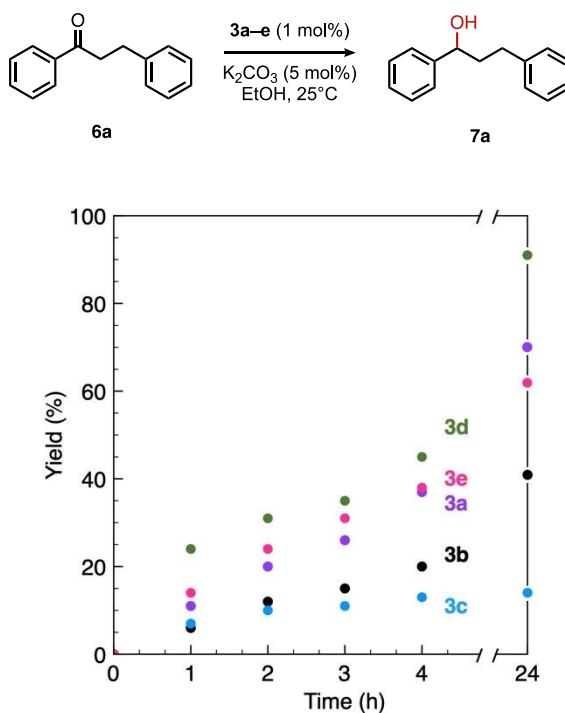

Figure 6. Time-conversion profiles for the transfer hydrogenation of 1,3-diphenylpropan-1-one **6a** using EtOH as hydrogen source under standard conditions catalyzed by complexes **3a–e**.

Table 4. Comparison of catalytic data for the transfer hydrogenation

of 1,3-diphenylpropan-1-one **5a** using complexes **3a–e**.[a]

entry	complex	TON
1	**3a**	70
2	**3b**	41
3	**3c**	14
4	**3d**	91
5	**3e**	62

[a] Reaction conditions: **5a** (0.5 mmol), K_2CO_3 (5 mol%), complex **3a–e** (1 mol%) in EtOH (5 mL), 25 °C, N_2; yields determined by ^1H NMR spectroscopy relative to 1,3,5-trimethoxybenzene from duplicate runs.

The activity of complex **3c** in transfer hydrogenation of C=C bonds is remarkable. The observed rates are orders of magnitude lower than the best Ru-based catalysts for transfer hydrogenation of C=O bonds,[45–47] yet considerably higher than that of unactivated C=C bonds.[48,49] As a consequence, catalysts generally afford allylic alcohols or fully saturated alcohols when exposed to α,β-unsaturated ketone substrates.[31,50–54] From a synthetic point, therefore, the pronounced selectivity towards C=C over C=O bonds in enone substrates is most remarkable and offers interesting synthetic opportunities.

High selectivity for olefin transfer hydrogenation of α,β-unsaturated ketones was observed when using complex **3c** with the bulkier substrate **5b** (Table 5, entries 1, 2). Within 4 h complete and selective hydrogenation of the olefinic C=C bond was observed with full retention of the C=O bond. After 24 h, the selectivity was 93% and thus still very high. Also, aliphatic enones such as cyclohexanone were converted welll (entry 3), which may point to electronic rather than π stacking effects that control the selectivity of complex **3c** (entry 3). Of note, selectivity and activity of the catalyst is substrate-dependent. For example, substrate **5d** was converted with both, complexes **3a** and **3c** well, though the selectivity was considerably better for complex **3a** (entry 4). Likewise, when using the conjugated diene **5e** as a substrate, conversion was considerably reduced and reached only 48% after 4 h, with a maximum yield of 40% of compound **6e** together with a mixture of isomerized products (entry 5). Longer reaction times did not improve the yield but instead only led to an increase of isomerized products. Similar isomerization side reactions were observed with complex **3a**, however conversion was almost complete and 73% yield of product **6c** were obtained already

after 3 h (entry 3). Even though complex **3c** is highly selective towards hydrogenation of the olefin bond in

α,β-unsaturated ketones with good retention of selectivity over time (entries 1–2), complex **3a** is preferred for

the conjugated dienone substrate **5c**. These data suggest that acyl group modification offers a useful strategy

for optimizing the catalyst towards high conversion of a specific substrate.

Table 5. Application of complex **3c** in transfer hydrogenation of unsaturated ketones **5a–e**. [a]

entry	substrate	product	time	conversion	yield
1	5a	6a	2 h	98%	98%
			24 h	>99%	98%
2	5b	6b	4 h	>99%	99%
			24 h	>99%	93%
3	5c	6c	2 h	92%	92%
4	5d	6d	6 h	83%	61%
			6 h [b]	84%	84%
5	5c	6c	4 h	52%	40%
			24 h	59%	39%
			3 h [b]	94%	73%

[a] reaction conditions: substrate (0.5 mmol), K_2CO_3 (5 mol%), complex **3c** (1 mol%) in EtOH (5 mL), 25 °C, N_2; yields determined by ^1H NMR spectroscopy relative to 1,3,5-trimethoxybenzene and average of duplicate runs; [b] using complex **3a** instead of **3c**.

Conclusions

Dalton Transactions Accepted Manuscript

In this work, we presented a series of N,N'-bidentate PYA ruthenium complexes as efficient catalysts for the selective olefin transfer hydrogenation of α,β-unsaturated ketones using ethanol as hydrogen source. Particularly, the introduction of a *para*-CF$_3$-substituted aryl group in the ligand acyl unit drastically improved the selectivity toward olefin hydrogenation, providing almost exclusively the desired ketone product with only minimal traces of the saturated alcohol even after extended reaction periods. The general adaptability of the bidentate ligand, with dynamic metal stabilization through π-acidic quinoidal and π-basic anionic forms constitutes an attractive platform for further catalytic applications, especially when the electronic nature of the metal-bound substrates and intermediates change throughout a catalytic cycle.

Experimental

General. All reactions were performed under air unless stated otherwise. Experiments under inert atmosphere were carried out using standard Schlenk techniques under N$_2$ atmosphere and dry deoxygenated solvents. The synthesis of ligands **2a–2e** are described in the ESI. Complex **3a** was prepared according to literature procedures.[18] Dry solvents were taken from a solvent purification system (SPS), stored over molecular sieves for at least 2 days, and degassed by N$_2$ gas bubbling for 30 min. All other compounds were commercially available and used as received. Nuclear magnetic resonance spectra were recorded on a Bruker Avance Neo spectrometer operating at 300 or 400 MHz for ^{1}H at room temperature unless otherwise noticed. All chemical shifts (d) are quoted in ppm and coupling constants in Hz. Chemical environments have been assigned through COSY, HSQC/HMBC or NOE NMR spectroscopic experiments. Residual protio solvent resonances were used as an internal reference for ^{1}H and ^{13}C{^{1}H} NMR spectra, and externally referenced to SiMe$_4$. ^{31}P{^{1}H} NMR spectra were referenced externally to 85% H$_3$PO$_4$ (D$_2$O). ^{19}F{^{1}H} NMR chemical shifts are externally referenced to CFCl$_3$. Elemental analyses were performed at the DCBP Microanalytic Laboratory using a Thermo Scientific Flash 2000 CHNS-O elemental analyzer. High-resolution mass spectrometry was carried out with a Thermo Scientific LTQ Orbitrap XL (ESI-TOF) by the DCBP mass spectrometry group at the University of Bern. UV-vis spectra were collected on Shimadzu UV 1800 Spectrophotometer, with a silicon

photodiode detector ranging from 190 to 1100 nm. Starna Scientific quartz cuvettes (type 23-N/Q/10) with a

path length of 10 mm were used. The spectra were collected at 298 K.

Synthesis of complex 3b. Compound **2b** (107 mg, 0.25 mmol), NaOAc (101 mg, 1.23 mmol) and

$[RuCl_2(cym)]_2$ (75 mg, 0.13 mmol) were dissolved in CH_2Cl_2 (10 mL). The reaction mixture was refluxed

for 16 h, cooled, and filtered through Celite. The filtered solution was washed with saturated $NaHCO_3$

solution (3 × 10 mL). The organic phase was dried over Na_2SO_4, filtered, and evaporated to dryness.

The crude product was purified by gradient column chromatography (neutral Al_2O_3; CH_2Cl_2 to

CH_2Cl_2/MeOH 99:1) to give analytically pure **3b** as a red solid (128 mg, 78%). ^1H NMR (CD_2Cl_2, 298K,

300 MHz): δ 9.90 (bs, 1H, NH), 8.55 (s, 1H, CH_{PYA}), 7.34 (dd, J = 6.9, 1.7 Hz, 1H, CH_{PYA}), 7.25 (d, J =

6.8 Hz, 1H, CH_{PYA}), 7.17 (d, J = 2.4 Hz, 2H, CH_{Ar}), 6.78 (t, J = 2.3 Hz, 1H, CH_{Ar}), 5.36 (d, J = 6.2 Hz,

2H, CH_{cym}), 5.14 (d, J = 6.2 Hz, 2H, CH_{cym}), 3.90 (s, 6H, 2 × OCH_3), 3.86 (s, 3H, NCH_3), 2.43 (septet, J

= 6.9 Hz, 1H, $CHMe_2$), 2.06 (s, 3H, cym-CH_3), 1.15 (d, J = 6.9 Hz, 6H, $CH(CH_3)_2$). $^{13}C\{^1H\}$ NMR (CD_2Cl_2,

298 K, 75 MHz): δ 182.12 (C=O), 161.24 (C_{Ar}), 160.99 (C_{PYA}), 142.34 (C_{Ar}), 140.94 (C_{PYA}), 133.29

(CH_{PYA}), 129.65 (CH_{PYA}), 110.34 (CH_{PYA}), 108.24 (CH_{Ar}), 104.29 (CH_{Ar}), 100.90 (C_{cym}), 92.10 (C_{cym}),

82.09 (CH_{cym}), 79.41 (CH_{cym}), 56.24 (OCH_3), 46.42 (NCH_3), 32.09 ($CHMe_2$), 23.36 ($CH(CH_3)_2$), 19.96

(cym-CH_3). $^{19}F\{^1H\}$ NMR (CD_2Cl_2, 298 K, 282 MHz): δ −72.44 (d, J = 711 Hz, PF_6). $^{31}P\{^1H\}$ NMR (CD_3CN,

298 K, 121 MHz): −144.17 (septet, J = 711 Hz, PF_6). HR-MS ESI: 522.1313 (522.1325 calcd. for [M–

PF_6]$^+$). Elem. Anal. found (calcd.) for $C_{25}H_{30}F_6N_3O_3PRu$: C 45.82 (45.05), H 4.52 (4.54), N 6.19 (6.30)%.

Synthesis of complex 3c. Compound **2c** (67 mg, 0.15 mmol), NaOAc (61 mg, 0.75 mmol), $[RuCl_2(cym)]_2$

(46 mg, 0.07 mmol) and $NaPF_6$ (63 mg, 0.37 mmol) were dissolved in CH_2Cl_2 (10 mL). The reaction

mixture was refluxed for 16 h, cooled, and filtered through Celite. The filtrate was washed with saturated

$NaHCO_3$ solution (3 × 5 mL). The organic phase was dried over Na_2SO_4, filtered, and evaporated to

dryness. The crude product was purified by gradient column chromatography (neutral Al_2O_3; CH_2Cl_2 to

CH_2Cl_2/MeOH 99:1) to give complex **3c** as a red solid (71 mg, 70%). Recrystallization from CH_2Cl_2 and

Et_2O afforded analytical pure material. ^1H NMR (CD_2Cl_2, 298K, 300 MHz): δ 10.13 (bs, 1H, NH), 8.57

(s, 1H, CH_{PYA}), 8.18 (d, J = 8.0 Hz, 2H, CH_{Ar}), 7.90 (d, J = 8.1 Hz, 2H, CH_{Ar}), 7.38 (dd, J = 6.9, 1.7 Hz,

1H, CH$_{PYA}$), 7.30 (d, J = 6.9 Hz, 1H, CH$_{PYA}$), 5.30 (d, J = 6.2 Hz, 2H, CH$_{cym}$), 5.11 (d, J = 6.2 Hz, 2H, CH$_{cym}$), 3.87 (s, 3H, NCH$_3$), 2.42 (septet, J = 6.9 Hz, 1H, CHMe$_2$), 2.06 (s, 3H, cym-CH$_3$), 1.15 (d, J = 6.9 Hz, 6H, CH(CH_3)$_2$). ^{13}C{^{1}H} NMR (CD$_2$Cl$_2$, 298 K, 75 MHz): δ 181.11 (C=O), 161.13 (C$_{PYA}$), 143.90 (C$_{Ar}$), 140.70 (C$_{PYA}$), 133.74 (CH$_{PYA}$), 130.35 (CH$_{Ar}$), 130.10 (CH$_{PYA}$), 125.94 (q, J = 4.0 Hz, CH$_{Ar}$), 110.60 (CH$_{PYA}$), 101.13 (C$_{cym}$), 91.84 (C$_{cym}$), 81.99 (CH$_{cym}$), 79.33 (CH$_{cym}$), 46.51 (NCH$_3$), 32.12 (CHMe$_2$), 23.33 CH(CH_3)$_2$, 20.00 (cym-CH$_3$). ^{19}F{^{1}H} NMR (CD$_2$Cl$_2$, 298 K, 282 MHz): δ –63.14 (s, CF$_3$), –72.13 (d, J = 711 Hz, PF$_6$). ^{31}P{^{1}H} NMR (CD$_3$CN, 298 K, 121 MHz): δ –144.11 (septet, J = 711 Hz, PF$_6$). HR-MS ESI: 530.0976 (530.0988 calcd. for [M–PF$_6$]$^+$). Elem. Anal. found (calcd.) for C$_{24}$H$_{25}$F$_9$N$_3$OPRu × 0.5 Et$_2$O: C 44.06 (43.89), H 3.91 (4.25), N 5.97 (5.01)%.

Synthesis of complex 3d. Complex **3d** was prepared in a procedure analogous to that described for **3c** starting from compound **2d** (144 mg, 0.33 mmol), NaOAc (138 mg, 1.68 mmol), [RuCl$_2$(cym)]$_2$ (103 mg, 0.17 mmol) and NaPF$_6$ (141 mg, 0.84 mmol). Complex **3d** was obtained as a red solid (152 mg, 68%). ^{1}H NMR (CD$_2$Cl$_2$, 298K, 300 MHz): δ 10.11 (bs, 1H, NH), 9.22 (s, 1H, CH$_{PYA}$), 8.20 (d, J = 8.2 Hz, 1H, CH$_{Ar}$), 8.16 (d, J = 8.2 Hz, 1H, CH$_{Ar}$), 8.07 (d, J = 7.7 Hz, 1H, CH$_{Ar}$), 7.97 (d, J = 7.1, 1H, CH$_{Ar}$), 7.74–7.58 (m, 3H, CH$_{Ar}$), 7.42 (dd, J = 6.8, 1.8 Hz, 1H, CH$_{PYA}$), 7.29 (d, J = 6.8 Hz, 1H, CH$_{PYA}$), 5.07 (br s, 1H, CH$_{cym}$), 4.89 (br s, 1H, CH$_{cym}$), 4.60 (br s, 2H, CH$_{cym}$), 3.92 (s, 3H, NCH$_3$), 2.11 (septet, J = 6.9 Hz, 1H, CHMe$_2$), 1.71 (s, 3H, cym-CH$_3$), 1.04 (d, J = 6.9 Hz, 6H, CH(CH_3)$_2$). ^{13}C{^{1}H} NMR (CD$_2$Cl$_2$, 298 K, 75 MHz): δ 182.85 (C=O), 161.44 (C$_{PYA}$), 140.03 (C$_{Ar}$), 139.82 (C$_{PYA}$), 134.08 (CH$_{PYA}$), 133.97 (C$_{Ar}$), 131.69 (CH$_{PYA}$), 131.57 (CH$_{Ar}$), 131.50 (C$_{Ar}$), 129.24 (CH$_{Ar}$), 127.99 (CH$_{Ar}$), 127.50 (CH$_{Ar}$), 127.33 (CH$_{Ar}$), 126.14 (CH$_{Ar}$), 125.31 (CH$_{Ar}$), 110.38 (CH$_{PYA}$), 100.19 (C$_{cym}$), 91.30 (C$_{cym}$), 82.03 (CH$_{cym}$), 79.24 (CH$_{cym}$), 46.58 (NCH$_3$), 31.83 (CHMe$_2$), 23.32 (CH(CH_3)$_2$), 19.71 (cym-CH$_3$). ^{19}F{^{1}H} NMR (CD$_2$Cl$_2$, 298 K, 282 MHz): δ –72.17 (d, J = 712 Hz, PF$_6$). ^{31}P{^{1}H} NMR (CD$_3$CN, 298 K, 121 MHz): δ –144.10 (septet, J = 712 Hz, PF$_6$). HR-MS ESI: 512.1260 (512.1270 calcd. for [M–PF$_6$]$^+$). Elem. Anal. found (calcd.) for C$_{27}$H$_{28}$F$_6$N$_3$OPRu: C 49.34 (49.39), H 4.19 (4.30), N 6.21 (6.40)%.

Synthesis of complex 3e. Complex **3e** was prepared in a procedure analogous to that described for **3c** starting from compound **2e** (47 mg, 0.10 mmol), NaOAc (43 mg, 0.51 mmol), [RuCl$_2$(cym)]$_2$ (32 mg, 0.05

mmol) and NaPF$_6$ (44 mg, 0.25 mmol). Complex **3e** was isolated as a red solid (66 mg, 92%). ^{1}H NMR (CD$_2$Cl$_2$, 298K, 300 MHz): δ 10.02 (bs, 1H, NH), 8.94 (s, 1H, CH$_{PYA}$), 8.49–8.42 (m, 1H, CH$_{Ar}$), 8.39–8.31 (m, 1H, CH$_{Ar}$), 7.97 (d, J = 8.0 Hz, 1H, CH$_{Ar}$), 7.68–7.60 (m, 2H, CH$_{Ar}$), 7.38 (dd, J = 6.9, 1.7 Hz, 1H, CH$_{PYA}$), 7.28 (d, J = 6.9 Hz, 1H, CH$_{PYA}$), 7.00 (d, J = 8.0 Hz, 1H, CH$_{Ar}$), 5.15 (br s, 1H, CH$_{cym}$), 5.01 (br s, 1H, CH$_{cym}$), 4.77 (br s, 2H, CH$_{cym}$), 4.16 (s, 3H, OCH$_3$), 3.90 (s, 3H, NCH$_3$), 2.23 (septet, J = 6.7 Hz, 1H, CHMe$_2$), 1.81 (s, 3H, cym-CH$_3$), 1.07 (d, J = 6.9 Hz, 6H, CH(CH_3)$_2$). ^{13}C{^{1}H} NMR (CD$_2$Cl$_2$, 298 K, 75 MHz): δ 182.91 (C=O), 161.21 (C$_{PYA}$), 158.87 (C$_{Ar}$), 140.44 (C$_{PYA}$), 133.51 (CH$_{PYA}$), 132.93 (C$_{Ar}$), 131.04 (C$_{Ar}$), 130.53 (CH$_{Ar}$), 130.16 (CH$_{PYA}$), 128.59 (CH$_{Ar}$), 126.58 (CH$_{Ar}$), 126.09 (CH$_{Ar}$), 125.98 (C$_{Ar}$), 123.16 (CH$_{Ar}$), 110.34 (CH$_{PYA}$), 102.94 (CH$_{Ar}$), 100.52 (C$_{cym}$), 91.43 (C$_{cym}$), 81.87 (CH$_{cym}$), 79.20 (CH$_{cym}$), 56.47 (OCH$_3$), 46.50 (NCH$_3$), 31.94 (CHMe$_2$), 23.38 CH(CH$_3$)$_2$, 19.86 (cym-CH$_3$). ^{19}F{^{1}H} NMR (CD$_2$Cl$_2$, 298 K, 282 MHz): δ –72.37 (d, J = 711 Hz, PF$_6$). ^{31}P{^{1}H} NMR (CD$_3$CN, 298 K, 121 MHz): δ –144.14 (septet, J = 709 Hz, PF$_6$). HR-MS ESI: 542.1366 (542.1376 calcd. for [M–PF$_6$]$^+$). Elem. Anal. found (calcd.) for C$_{28}$H$_{30}$F$_6$N$_3$O$_2$PRu: C 48.87 (48.98), H 4.44 (4.40), N 5.61 (6.12)%.

General catalytic procedure: In a 10 mL round bottom flask, the substrate (0.5 mmol), complex **1** (1 mol%), 1,3,5-trimethoxybenzene or mesitylene (10 mol%, internal standard) were dissolved in EtOH (5 mL) and the solution was degassed with N$_2$ for 10 min. The catalytic run was started with the injection of K$_2$CO$_3$ (5 mol%, 2 M solution in H$_2$O) and the tube was placed in a thermostated oil bath (25 °C). The reaction was monitored by ^{1}H NMR spectroscopy by taking aliquots (ca. 0.1 mL) at set times under N$_2$, which were dissolved in CDCl$_3$ (0.5 mL) to determine the spectroscopic conversion and yields relative to the internal standard.

Crystal structure determination. A suitable crystal of **3b** was mounted and then transferred into a cold stream of nitrogen (173 K). All measurements were made on a *RIGAKU Synergy S* area-detector diffractometer using mirror optics monochromated Cu *K*α radiation (λ = 1.54184 Å). Data reduction was performed using the *CrysAlisPro*[55] program. The intensities were corrected for Lorentz and polarization effects, and an absorption correction based on the multi-scan method using SCALE3 ABSPACK in *CrysAlisPro*[55] was applied. The structure was solved by intrinsic phasing using *SHELXT*,[56] which revealed the positions of all non-hydrogen atoms. All non-hydrogen atoms were refined anisotropically. H-atoms were assigned in geometrically

calculated positions and refined using a riding model (1.2 Ueq of parent atom, 1.5 Ueq for methyl groups) except for the hydrogen atom attached to N1, which was located from the difference density map and had its position and isotropic displacement parameter refined freely. Refinement of the structure was carried out on F^2 using full-matrix least-squares procedures, which minimized the function $\Sigma w(F_o^2 - F_c^2)^2$. All calculations were performed using the *SHELXL-2014/7*[57] program in OLEX2.[58] Data collection and refinement parameters for **3b** are given in Table S13. Crystallographic data for this structure have been deposited with the Cambridge Crystallographic Data Centre (CCDC) as supplementary publication number 2422796.

Acknowledgments

Conflict of Interest

The authors declare no conflict of interest.

References

1   J. P. Collman, *Acc. Chem. Res.*, 1968, **1**, 136–143.

2   B. Cornils, W. A. Herrmann, M. Beller, R. Paciello, *Applied Homogeneous Catalysis with Organometallic Compounds* (3rd Ed), Eds. Wiley-VCH, Weinheim (Germany), 2017.

3   R. H. Crabtree, *The Organometallic Chemistry of the Transition Metals* (7th Ed), John Wiley & Sons Inc, Hoboken (USA) 2019.

4   R. B. Jordan, *Reaction Mechanisms of Inorganic and Organometallic Systems* (3rd Ed), Oxford University Press, New York (USA), 2007.

5   T. J. Johnson, K. Folting, W. E. Streib, J. D. Martin, J. C. Huffman, S. A. Jackson, O. Eisenstein and K.

Dalton Transactions Accepted Manuscript

G. Caulton, *Inorg. Chem.,* 1995, **34**, 488–499.

6   T. Gottschalk-Gaudig, K. Folting and K. G. Caulton, *Inorg. Chem.,* 1999, **38**, 5241–5245.

7   H. Nagashima, H. Kondo, T. Hayashida, Y. Yamaguchi, M. Gondo, S. Masuda, K. Miyazaki, K. Matsubara and K. Kirchner, *Coord. Chem. Rev.,* 2003, **245**, 177–190.

8   M. Jiménez-Tenorio, M. C. Puerta and P.Valerga, *Eur. J. Inorg. Chem.,* 2004, 17–32.

9   T. Glöge, K. Jess, T. Bannenberg, P. G. Jones, N. Langenscheidt-Dabringhausen, A. Salzer and M. Tamm, *Dalton Trans.,* 2015, **44**, 11717–11724.

10 E. R. Paulson, C. E. Moore, A. L. Rheingold, D. P. Pullman, R. W. Sindewald, A. L. Cooksy and D. B. Grotjahn, *ACS Catal.,* 2019, **9**, 7217–7231.

11 M. B. Kindervater, V. N. Staroverov, K. M. K. Jackman, A. A. Fogh, L. S. G. Kelley, L. Lim, S. A. Sirohey, P. D. Boyle and J. M. Blacquiere, *Dalton Trans.,* 2023, **52**, 10744–10750.

12 IUPAC Compendium of Chemical Terminology, 5th ed. International Union of Pure and Applied Chemistry; 2025. Online version 5.0.0, 2025. https://doi.org/10.1351/goldbook.C01334.

13 J. J. Race and M. Albrecht, *ACS Catal.,* 2023, **13**, 9891–9904.

14 N. Lentz and M. Albrecht, *ACS Catal.,* 2022, **12**, 12627–12631.

15 N. Lentz, S. Reuge and M. Albrecht, *ACS Catal.,* 2023, **13**, 9839–9844.

16 A. Beaufils, P. Melle, N. Lentz and M. Albrecht, *Inorg. Chem.,* 2024, **63**, 2072–2081.

17 N. Lentz, S. Reuge, A. Beaufils and M. Albrecht, *Organometallics,* 2024, **43**, 1536–1546.

18 M. Albrecht, A. Beaufils, *ChemCatChem,* 2025, **17**, e202401596.

19 M. E. Doster and S. A. Johnson, *Angew. Chem. Int. Ed.*, 2009, **48**, 2185–2187.

20 Q. Shi, R. J. Thatcher, J. Slattery, P. S. Sauari, A. C. Whitwood, P. C. McGowan, R. E. Douthwaite, *Chem. Eur. J.* **2009**, *15*, 11346–11360.

21 J. Slattery, R. J. Thatcher, Q. Shi and R. E. Douthwaite, *Pure Appl. Chem.*, 2010, **82**, 1663–1671.

22 P. D. W. Boyd, L. J. Wright and M. N. Zafar, *Inorg. Chem.,* 2011, **50**, 10522–10524.

23 T. Pfister, T. Söhnel, T. J. Collins and L. J. Wright, *Chem. Eur. J.*, 2023, **29**, e202301548.

24 N. S. Y. Abdolla, D. L. Davies and K. Singh, *Eur. J. Inorg. Chem.*, 2021, 939–950.

25 V. Leigh, D. J. Carleton, J. Olguin, H. Mueller-Bunz, L. J. Wright and M. Albrecht, *Inorg. Chem.,* 2014, **53**, 8054–8060.

26 M. Navarro, M. Li, H. Müller-Bunz, S. Bernhard and M. Albrecht, *Chem. Eur. J.,* 2016, **22**, 6740–6745.

27   M. Navarro, C. A. Smith and M. Albrecht, *Inorg. Chem.,* 2017, **56**, 11688–11701.

28   E. Reusser, M. Aeschlimann and M. Albrecht, *Cat. Sci. Technol.,* 2025, **15**, 867–877.

29   P. Melle, N. Ségaud and M. Albrecht, *Dalton Trans.,* 2020, **49**, 12662–12673.

30   V. Vigneswaran, S. N. MacMillan and D. C. Lacy, *Organometallics,* 2019, **38**, 4387–4391.

31   S. Horn, C. Gandolfi and M. Albrecht, *Eur. J. Inorg. Chem.,* 2011, 2863–2868.

32   T. Vielhaber and C. Topf, *Appl. Catal. A*, 2021, **623**, 118280.

33   T. Vielhaber, K. Faust, T. Bögl, W. Schöfberger and C. Topf, *J. Catal*., 2022, **416**, 352–363.

34   A. Abbotto, S. Bradamante and G. A. Pagani, *J. Org. Chem.,* 2001, **66**, 8883–8892.

35   K. Salzmann, C. Segarra and M. Albrecht, *Angew. Chem. Int. Ed.,* 2020, **59**, 8932–8936.

36   T. Zweifel, J.-V. Naubron, T. Büttner, T. Ott and H.Grützmacher, *Angew. Chem. Int. Ed.*, 2008, **47**, 3245–3249.

37   N. Castellanos-Blanco, A. Arévalo and J. J. García, *Dalton Trans.,* 2016, **45**, 13604–13614.

38   P. Weingart, Y. Sun and W. R. Thiel, *ChemCatChem* 2020, **12**, 6223–6233.

39   R. Ghosh, R. R. Behera, S. Panda, S. K. Behera, N. C. Jana and B. Bagh, *ChemCatChem* 2023, **15**, e202201062.

40   R. Ghosh, N. C. Jana, S. Panda and B. Bagh, *ACS Sustain. Chem. Eng.* 2021, **9**, 4903–4914.

41   C. Reichardt and T. Welton, *Solvents and Solvent Effects in Organic Chemistry*, Wiley-VCH, Weinheim, 2010.

42   W. Kaim, S. Kohlmann, S. Ernst, B. Olbrich-Deussner, C. Bessenbacher and A. Schulz, *J. Organomet. Chem.,* 1987, **321**, 215–226.

43   14% of alcohol product is considerably higher than the 2% obtained when starting from *trans*-chalcone, indicating some product inhibition when ketone **5a** is generated in situ. This has been observed previously with a pincer PYA Ru complex for the selective transfer hydrogenation of methyl cinnamylketone using iPrOH (see ref. 44). In the latter, deactivation of the catalytically active species was confirmed upon addition of acetophenone after full consumption of the substrate, resulting in negligeable 5% conversion after 6 h while full conversion is obtained in 0.5 h in a separate run.

44   P. Melle, Y. Manoharan and M. Albrecht, *Inorg. Chem.*, 2018, **57**, 11761–11774.

45   W. Baratta, M. Bosco, G. Chelucci, A. Del Zotto, K. Siega, M. Toniutti, E. Zangrando and P. Rigo, *Organometallics*, 2006, **25**, 4611–4620.

Dalton Transactions Accepted Manuscript

46   L. Pardatscher, B. J. Hofmann, P. J. Fischer, S. M. Hölzl, R. M. Reich, F. E. Kühn and W. Baratta, *ACS Catal.*, 2019, **9**, 11302–11306.

47   P. Melle, J. Thiede, D. Hey and M. Albrecht, *Chem. Eur. J.,* 2020, **26**, 13226–13234.

48   S. Horn and M. Albrecht, *Chem. Commun.,* 2011, **47**, 8802–8804.

49   I. D. Alshakova, B. Gabidullin and G. I. Nikonov, *ChemCatChem*, 2018, **10**, 4860–4869.

50   R. A. Farrar-Tobar, Z. Wei, H. Jiao, S. Hinze and J. G. de Vries, *Chem. Eur. J.*, 2018, **24**, 2725–2734.

51   T. Zweifel, J.-V. Naubron, T. Büttner, T. Ott and H. Grützmacher, *Angew. Chem. Int. Ed.*, 2008, **47**, 3245–3249.

52   R. D. Patil and S. Pratihar, *J. Org. Chem.*, 2024, **89**, 1361–1378.

53   For a Ni variant, see: P. Yang, H. Xu and J. Zhou, *Angew. Chem. Int. Ed.,* 2014, **53**, 12210–12213.

54   V. Vigneswaran, S. N. MacMillan and D. C. Lacy, *Organometallics*, 2019, **38**, 4387–4391.

55   CrysAlisPro (Version 1.171.40.37a). Oxford Diffraction Ltd., Yarnton, Oxfordshire (UK), 2018.

56   G. M. Sheldrick, *Acta Cryst.*, 2015, **A71**, 3-8.

57   G. M. Sheldrick, *Acta Cryst.*, 2015, **C71**, 3-8.

58   O. V. Dolomanov, L. J. Bourhis, R. J. Gildea, J. A. K. Howard and H. Puschmann, *J. Appl. Crystallogr.*, 2009, **42**, 339–341.

Dalton Transactions Accepted Manuscript

Data availability statement:

- The data supporting this article have been included as part of the Electronic Supplementary Information (ESI).
- Crystallographic data for compound **3b** has been deposited at the CCDC under No. 2422796 and can be obtained from https://www.ccdc.cam.ac.uk free of charge.

Dalton Transactions Accepted Manuscript